Experimentally and Numerically Analysis of Flow Behaviors in Grooved Channels for Pulsatile Flow

Zhichao XU[*1], Gang CAO[*1], Yongning BIAN[*2] and Hirofumi ARIMA[*3]

[*1,2] School of Ocean Science and Technology, Dalian University of Technology, 116024, China
[*3]Institute of Ocean Energy, Saga University, 840-8502, Japan

Abstract

In this paper, the flow behaviors in the rectangular grooved channel which is the basic unit of the plate heat exchanger is investigated. Under the action of the pulsating flow field, the flow characteristics and flow structure in different lengths of grooved channels are analyzed experimentally and numerically. The instantaneous pulsating flow rate is monitored by an electromagnetic flowmeter to analyze the change rule of the pulsation ratio of the pulsating flow in the experiment, and the overall pressure drop in the grooved channel is monitored by a differential transducer. Furthermore, the flow is visualized by the aluminum dust method. It is seen that the flow visualization method matched well with the numerical simulation results. In the grooved channels with different groove lengths, the pulsation ratio of the flow is influenced obviously by the frequency of pulsation. It can be observed that the actual pulsation ratio of the pulsating flow decreases with increasing frequency. In addition, it can be revealed that there is a phase difference between the curves of flow rate and pressure drop with time, and the magnitude of the phase difference is related to the pulsation frequency and the groove length.

Keywords: Grooved channel, Numerical simulation, Aluminum dust method, Real pulsation ratio, Phase difference

1.Introduction

Ocean thermal energy conversion (OTEC) is an essential method for utilizing ocean thermal energy. The basic principle of Ocean Thermal Energy Conversion (OTEC) is to use the warm water (26-28°C) on the ocean surface to heat and vaporize the work fluid in the circulating system, and the resulting steam drives the turbine to rotate and generate electricity. Deep cold seawater (4-6°C) condenses the exhaust gas into a liquid again and a thermodynamic cycle is completed (Weiming Liu et al., 2020).

In the ocean thermal energy conversion cycle, the high-efficiency plate heat exchanger is a crucial equipment. To study the plate heat exchanger, the rectangular groove channel is the basic unit. (Han Huang et al., 2018) carried out numerical and experimental studies on the grooved channel with different groove lengths and determined the groove length $l = 4mm$ for the maximum value of the heat transfer coefficient. (Fengge Zhang et al., 2019) studied the heat transfer efficiency of the grooved channel with different pulsation frequencies, and the results showed that the heat transfer efficiency increases with the increase of frequency, especially the smaller the amplitude of pulsation flow the better the heat transfer effect is at the low frequency. (Junxiu Pan et al., 2020) studied the heat transfer efficiency of grooved channels with different pulsation ratios. The maximum heat transfer enhancement factor is 2.74 when the pulsation ratio is 1.4, which suggests that the pulsating flow with reverse flow can increase the heat transfer.

2. Numerical simulation and experiment

2.1 Experimental settings

[*] Date of Manuscript Acceptance 2023.12.28
E-mail of corresponding author: ybian@dlut.edu.cn

The experimental setup is depicted in Fig. 2.1 (a) below. Water is utilized as the working medium and all experiments are conducted at room temperature. The water tank is used for water storage and the water as the working medium is sent to the test section by a centrifugal pump. The volumetric flow rate of water is adjusted by a control valve. The pulsating flow in the experiment is obtained utilizing a piston pump, which is driven by a servo motor. The flow rate of the mass was measured by an electromagnetic flowmeter with a measurement error of $1\ ml/s$. The total differential pressure in the test section was measured by a micro-pressure manometer with a measurement error of $0.065\ kPa$. In addition, the flow visualization was done by using the aluminum dust method to observe the flow structure of the fluid in the groove.

The photographing system is shown in Fig. 2.1 (b) below. Aluminum dust particles with a diameter of about $40\ \mu m$ are injected into the circulating pipeline. The flow lines in the observation section can be observed through the reflection of the aluminum dust on the light source. Since the instantaneous velocity flow field repeats periodically after the fully developed section, the groove of the 20th cycle was chosen as the observation section in this experiment. A cold light sheet was used as the light source, and the flow lines in the groove were photographed with a light-controlled digital camera.

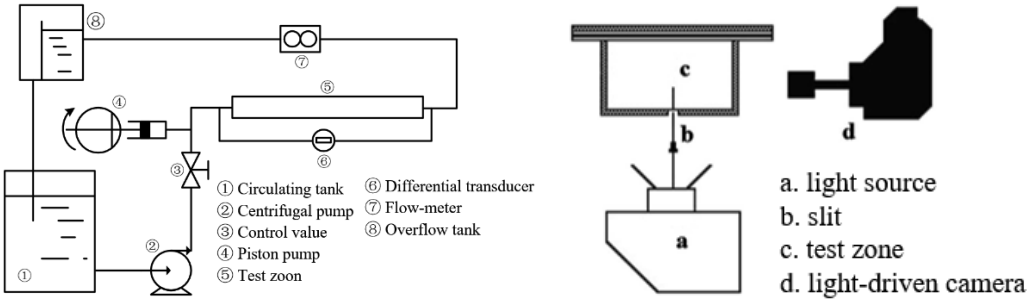

(a) Diagram of the experimental system. (b) Diagram of the photographing system.

Fig.2.1 Experimental system and Photographing system.

The structure of the groove is shown in Fig. 2.2 below. h^*, f^*, and $t^*$are the characteristic length, the frequency of the pulsating flow, and the time, respectively, and in this paper $l^* = 8, 10, 12$, and the physical quantities are labelled with "*" in the upper right corner to indicate that they are dimensioned values.

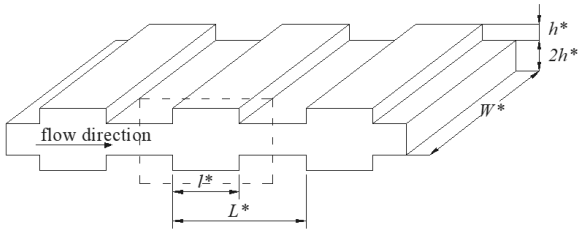

Fig.2.2 Structure of the grooved channel.

The average velocity at the inlet of the grooved channel is:

$$u_s^* = Q_s^* / (2W^* h^*) \tag{1}$$

where Qs* is the volume flow rate of the constant flow.

As suggested by (Faming Sun et al., 2010), the characteristic velocity of the pulsatile flow $u_m{}^*$ is calculated by:

$$u_m^* = 3/2 \bullet u_s^* \tag{2}$$

The net Reynolds number is calculated as:

$$Re_s = \rho^* u_m^* h^* / \mu^* \tag{3}$$

where μ^* and ρ^* are the viscosity and density of water, respectively.

The amplitude $Q_0{}^*$ of the pulsating flow volume flow rate is:

$$Q_0^* = 2\pi f^* s^* (\pi D_p^{*2} / 4) \tag{4}$$

where s^* is the stroke of the piston pump and the diameter of the piston $D_p{}^* = 50$ mm.

The pulsation ratio P is the ratio of the amplitude of the pulsating flow volume flow rate to the net flow rate:

$$P = Q_0^* / Q_s^* \tag{5}$$

The instantaneous volume flow rate $Q_i{}^*$ is:

$$Q_i^* = Q_s^* + Q_0^* \sin(2\pi f^* t^*) = Q_s^* [1 + P \sin(2\pi f^* t^*)] \tag{6}$$

2.2 Numerical simulation method

According to (Adachi and Uehara, 2001b), it was shown that the instantaneous velocity field repeats periodically in the fully developed region. The flow reaches the fully developed state at the 9th groove from the inlet boundary. Considering that the current research situation is also in this flow state, a model consisting of 25 basic units of typical rectangular grooves was used. A structured grid was used in this study as shown in Fig. 2.3. It should be explained that an extended straight pipe was added at the exit of the fluted channel in order to minimize the influence of the exit boundary on the flow inside the groove.

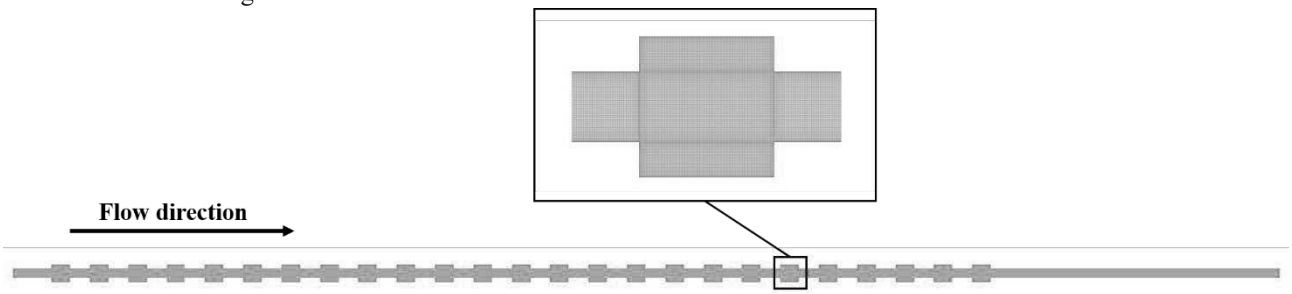

Fig.2.3 Schematic of the grid in the grooved channel.

In this study, the finite volume method (FVM) numerical method is used to investigate the flow characteristics and heat transfer characteristics in the grooved channel. The commercial software ANSYS Fluent is used for the numerical simulation of the flow procedure. The Reynolds number $Re = 500$ was chosen for the numerical simulation, which is lower than the critical Reynolds number $Re_c = 604$ (Faming Sun et al., 2010), which indicates that the flow state in the flow path is still laminar during the pulsation period. Therefore, the laminar flow model is chosen for this simulation. The coupling of pressure and velocity is performed using the SIMPLE algorithm. The solution is considered to be converged when the normalized residuals reach 10^{-8} for the energy equation and 10^{-6} for the continuity and velocity equations. The boundary conditions at the inlet of the flow channel were set as velocity inlet and pulsation flow was realized through the prepared UDF, the outlet was set as pressure outlet, the upper and lower walls of the groove were set as constant temperature and set as the no-slip wall.

The grooved channel was modelled using a dimensionless method, where each physical quantity was dimensioned as:

$$x = x^* / h^*, y = y^* / h^*, u = u^* / u_m^*, v = v^* / v_m^*, p = p^* / (\rho^* u_m^{*2}), T = (T^* - T_{in}^*) / (T_w{}^* - T_{in}^*) \tag{7}$$

Where u^* is the flow rate in the horizontal coordinate direction, v^* is the flow rate in the vertical coordinate direction, p^* is the pressure difference, T^* is the temperature of the local work material, $T_w{}^*$ is the temperature of the wall of the recessed channel, and $T_{in}{}^*$ is the inlet temperature of the work material.

Then the dimensionless governing equations can be written as:

$$\frac{\partial u}{\partial x} + \frac{\partial v}{\partial y} = 0 \tag{8}$$

$$St\frac{\partial u}{\partial t}+u\frac{\partial u}{\partial x}+v\frac{\partial u}{\partial y}=-\frac{\partial p}{\partial x}+\frac{1}{Re}(\frac{\partial^2 u}{\partial x^2}+\frac{\partial^2 u}{\partial y^2})$$

$$St\frac{\partial v}{\partial t}+u\frac{\partial v}{\partial x}+v\frac{\partial v}{\partial y}=-\frac{\partial p}{\partial y}+\frac{1}{Re}(\frac{\partial^2 v}{\partial x^2}+\frac{\partial^2 v}{\partial y^2}) \tag{9}$$

$$St\frac{\partial T}{\partial t}+u\frac{\partial T}{\partial x}+v\frac{\partial T}{\partial y}=\frac{1}{RePr}(\frac{\partial^2 T}{\partial x^2}+\frac{\partial^2 T}{\partial y^2}) \tag{10}$$

Where Pr is the Prandtl number.

St number (Strouhal number) is calculated as:

$$St=f^*h^*/u_m^* \tag{11}$$

3. Results and discussions

3.1 Numerical simulation results

When $p=1.4, Re=500, St=0.1765$, the flow structure images inside the fully developed groove at eight moments in the numerical simulation are compared with the experimental images, as shown in Fig. 3.1 below.

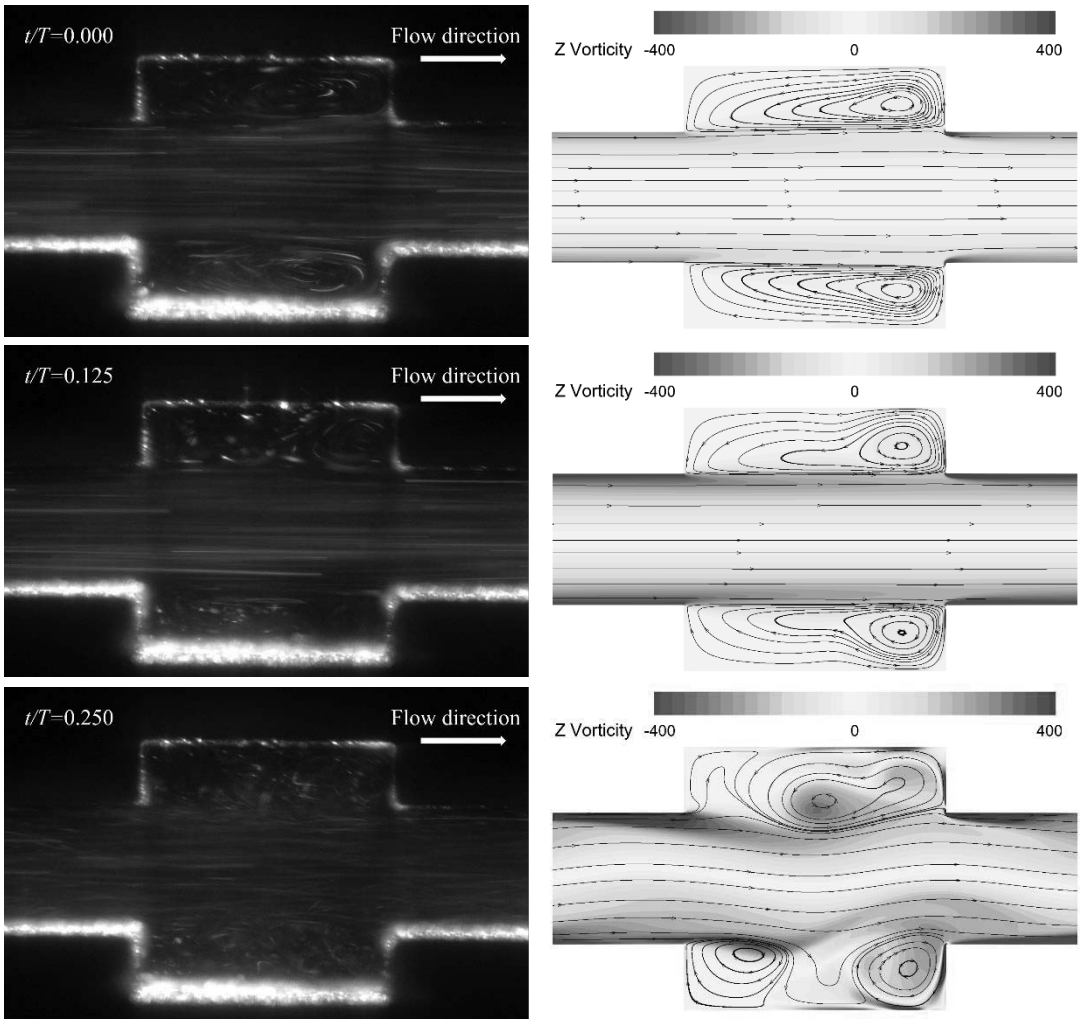

Fig.3.1 Comparison between numerical and experimental vortex structure.

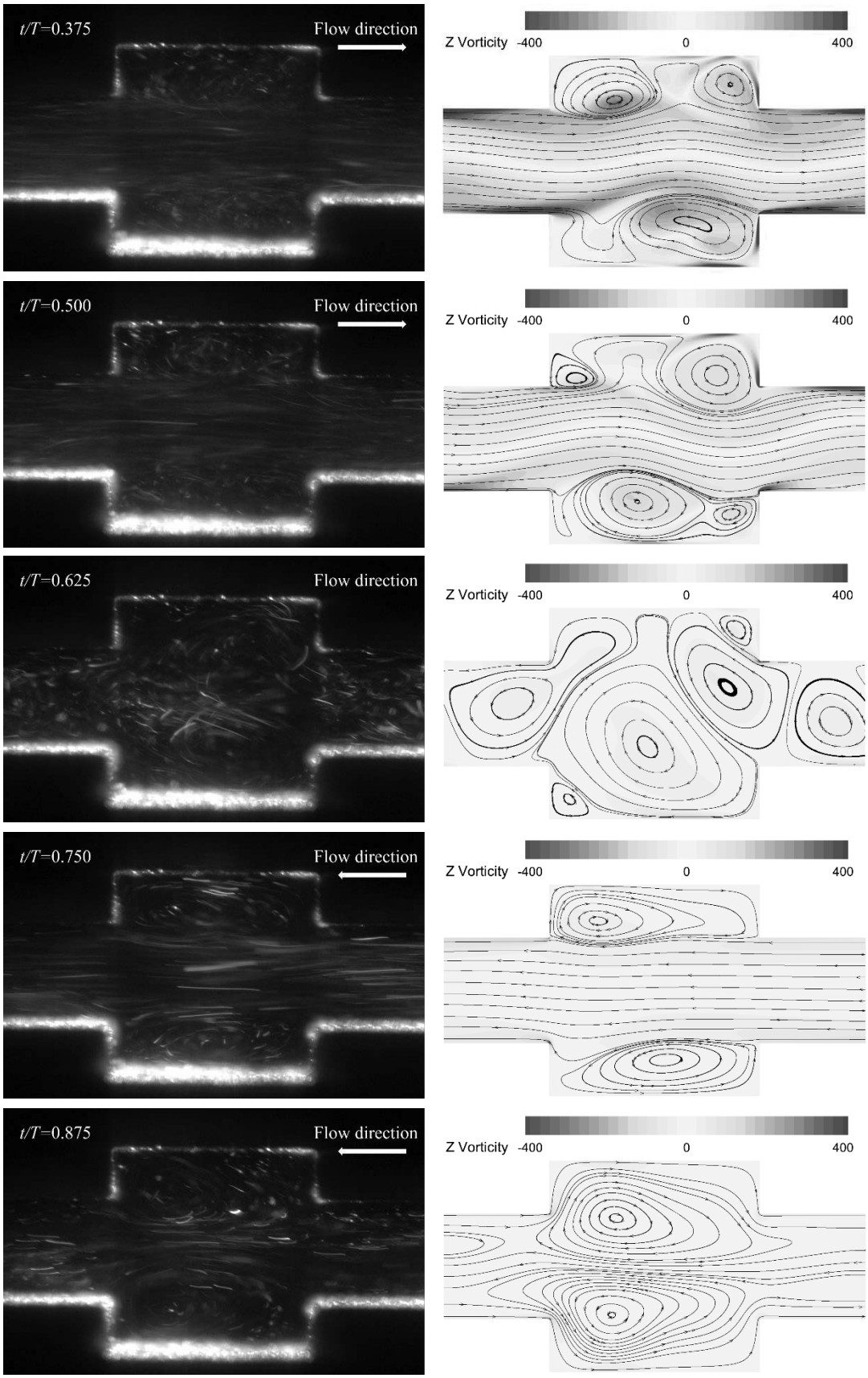

Fig.3.1 Continued.

It can be observed that the vortex structure inside the groove in the numerical simulation results matches the vortex structure in the experiments at different moments well within a pulsation period, which proves that the numerical method adopted in this paper is reasonable and correct. Therefore, the numerical simulation method can be applied in different structural grooved channels.

3.2 Experimental results and discussions

3.2.1 The practical pulsation ratio

In the experiments, the practical pulsation ratio of the pulsation flow is not the same as the set pulsation ratio P. Therefore, the relationship between the actual and set values of the pulsation ratio is analyzed in depth. Define O_f to reflect the real amplitude of the pulsation flow in the experiment, and its calculation formula is:

$$O_f = \frac{Q_e^*}{Q_s^*} \tag{12}$$

Where Q_e^* is the maximum value of pulsating flow in the experiments.

The O_f at different St numbers for groove lengths $l^* = 8, 10, 12$ with $Re = 375$ and pulsation ratios $p = 0.6$, 1.0, 1.4 have been analyzed respectively, as shown in Figs. 3.2. It can be observed that O_f decreases gradually with the increase of the St number, which can indicate that the gap between the practical and theoretical values of the pulsation ratio increases with the increase of pulsation frequency. Therefore, the actual pulsation ratio is closer to the set value of the pulsation ratio when the experiment is carried out under low-frequency conditions. Where from the figure, the groove length has less effect on the practical pulsating ratio.

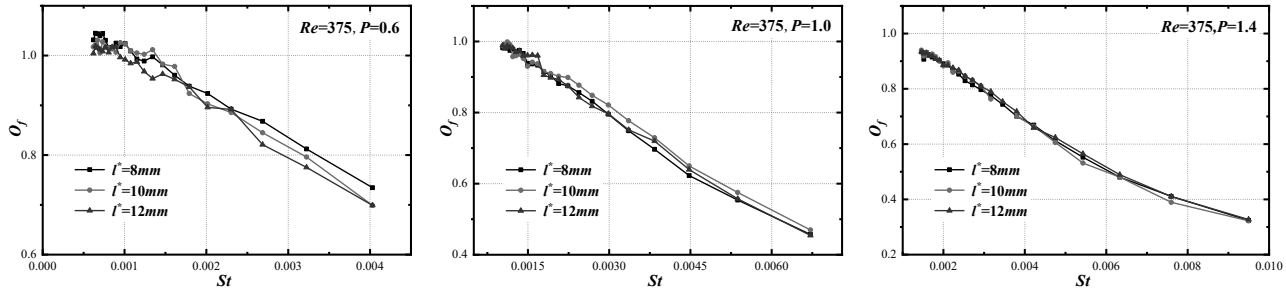

(a) (b) (c)

Fig.3.2 Practical pulsation ratio of experimental data.

3.2.2 The phase difference

In the experiments, there is a significant phase difference between the instantaneous flow curve and the pressure drop curve, as shown in Fig. 3.3 below, and it varies with the experimental conditions.

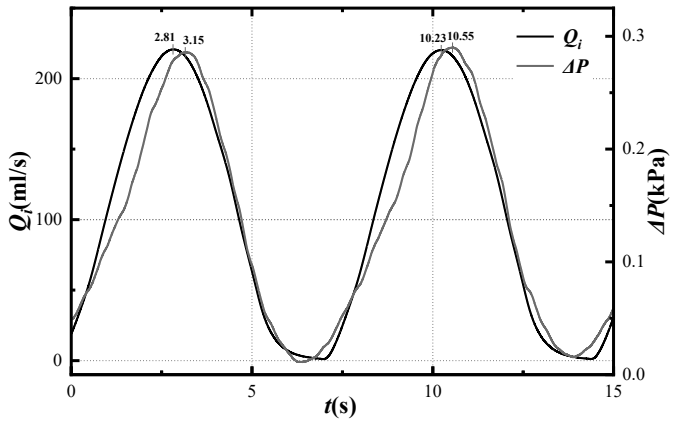

Fig.3.3 Phase difference between flow rate and pressure drop.

The phase difference $\Delta\varphi$ is defined as the difference in acquisition time corresponding to the extreme values of the pressure drop and flow curves, with the expression:

$$\Delta\varphi = 360^{\circ}\left(t_{\Delta P} - t_{Q_i}\right) f \tag{13}$$

The phase difference for different pulsation ratios and different St numbers for groove lengths $l^* = 8, 10, 12$ at $Re = 375$ have been analyzed, as shown in Fig. 3.4. Overall, the phase difference for different pulsation ratios decreases with the increase of pulsation frequency, but it tends to decrease and then increases in the case of pulsation ratio $p = 1.4$. With the increase in frequency, the peak of the pressure drop will be ahead of the peak of the flow wave, forming a negative phase difference. It is also found that at different frequencies, the phase difference is always the largest for groove length $l^* = 12$ and always the smallest for $l^* = 8$, so it can be concluded that the magnitude of the phase difference is not only related to the frequency but also to the length of the groove.

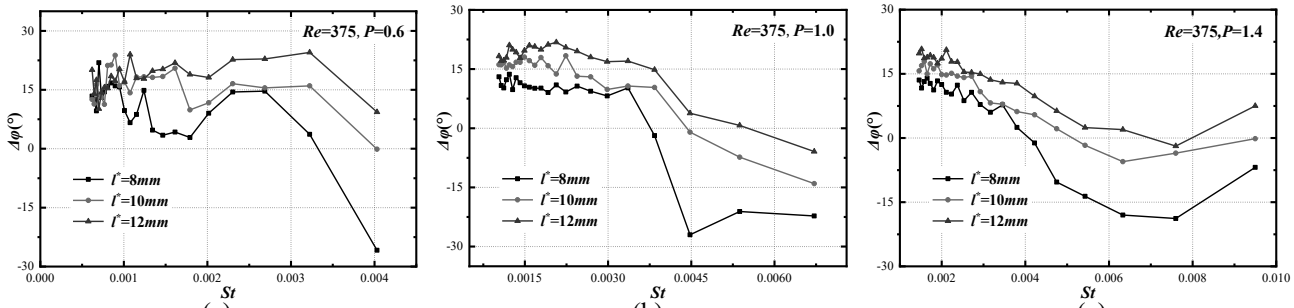

Fig.3.4 Phase difference of experimental data.

4. Conclusions

In this paper, a combination of experimental and numerical simulation is used to investigate the grooved channel under a pulsating flow field. The following main conclusions can be drawn.

(1) The vortex structure post-processing image obtained by the numerical simulation method matches well with the experimental flow visualization vortex structure image, which indicates that the numerical simulation method used in this study is reasonable, and this method can be applied to different structures in the grooved channel.

(2) The experimental results show that the groove structure has less influence on the real pulsation ratio, and the gap between the real pulsation ratio and the theoretical pulsation ratio increases with the increase of pulsation frequency.

(3) From the experiments, the magnitude of the phase difference decreases with the increase of pulsation frequency, and the peak of the pressure drop will be ahead of the peak of the flow wave, forming a negative phase difference. The longer the length of the groove the larger the phase difference.

Acknowledgments

This study is sponsored by the National Key R&D Program of China (2019YFB1504301), and the Cooperative Research Program of IOES (No. 23A13).

References

Takahiro Adachi, Haruo Uehara. Correlation between heat transfer and pressure drop in channels with periodically grooved parts [J]. International Journal of Heat and Mass Transfer,2001,44(22):

Faming Sun, Yongning Bian and Hirofumi Arima. Strength characteristics of the self-sustained wave in grooved channels with different groove length [J]. Heat Mass Transfer (2010) 46:1229–1237:

Han Huang, Yongning Bian. Numerical and experimental analysis of heat transfer enhancement and pressure drop characteristics of laminar pulsatile flow in grooved channel with different groove lengths [J]. Applied Thermal Engineering 137 (2018) 632–643:

Fengge Zhang, Yongning Bian and Yang Liu. Experimental and numerical analysis of heat transfer enhancement and flow characteristics in grooved channel for pulsatile flow [J]. International Journal of Heat and Mass Transfer 141 (2019) 1168–1180:

Junxiu Pan, Yongning Bian and Yang Liu. Characteristics of flow behavior and heat transfer in the grooved channel for pulsatile flow with a reverse flow [J]. International Journal of Heat and Mass Transfer 147 (2020) 118932:

Weimin Liu, Xiaojian Xu and Fengyun Chen. A review of research on the closed thermodynamic cycles of ocean thermal energy conversion [J]. Renewable and Sustainable Energy Reviews 119 (2020) 109581: